

# Discovering Dynamic Symbolic Policies with Genetic Programming

Sigur de Vries<sup>1\*</sup>, Sander Keemink<sup>1</sup>, and Marcel van Gerven<sup>1</sup>

<sup>1</sup>Department of Machine Learning and Neural Computing, Donders Institute for Brain, Cognition and Behaviour, Radboud University, Nijmegen, the Netherlands

\*sigur.devries@ru.nl

## Abstract

Artificial intelligence techniques are increasingly being applied to solve control problems, but often rely on black-box methods without transparent output generation. To improve the interpretability and transparency in control systems, models can be defined as white-box symbolic policies described by mathematical expressions. While current approaches to learn symbolic policies focus on static policies that directly map observations to control signals, these may fail in partially observable and volatile environments. We instead consider dynamic symbolic policies with memory, optimised with genetic programming. The resulting policies are robust, and consist of easy to interpret coupled differential equations. Our results show that dynamic symbolic policies compare with black-box policies on a variety of control tasks. Furthermore, the benefit of the memory in dynamic policies is demonstrated on experiments where static policies fall short. Overall, we present a method for evolving high-performing symbolic policies that offer interpretability and transparency, which lacks in black-box models.

## 1 Introduction

Many problems in our increasingly complex society can be viewed as control problems, where the goal is to make optimal decisions in real time such as to regulate the behaviour of the controlled system, ranging from smart infrastructure systems to healthcare systems [3]. In recent years, there have been many successful applications of artificial intelligence (AI) to control problems, offering automated solutions to regulate complex non-linear processes. While the employed control algorithms achieve high performance, they usually require the use of black-box models such as neural networks [1]. Such black-box models often allow for highly general computations, but lack interpretability of their functioning, making it difficult to understand the computed decisions and actions [27]. Transparency is particularly important in control systems, because it aids in identification of biases, fault detection and improvement and could therefore raise confidence of users in the system’s reliability [47].

In contrast to black-box models, white-box models allow for easy inspection of their internal mechanisms [1]. However, white-box models show an accuracy-interpretability trade-off and there are currently no general training methods to produce white-box approaches that can compete with black-box approaches in terms of efficiency and accuracy [27, 31]. Most white-box approaches opt for post-training model distillation to produce a transparent model that learns the input-output mapping of a black-box model [13]. Disadvantages of model distillation are that it requires a two-phase learning process and information loss could occur in the distillation phase [34]. Therefore, it may be more desirable to learn white-box models directly. When training an inherently white-box model, interpretability of decisions already occurs at intermediate stages, showing transparent learning, and outputs are directly dependent on explainable features [34].

A promising candidate for white-box control systems are symbolic policies [8, 26, 13]. Symbolic policies are described by interpretable symbolic expressions, consisting of mathematical operators and state variables. Similar to symbolic regression [6], symbolic policy learning does not require a predefined model structure, therefore it is less affected by human bias or knowledge gaps compared to other data-driven approaches. Additionally, symbolic policies may capture rules that generalise better to other settings, and learned equations tend to be more efficient than neural networks in terms of parameter count [26].

Current approaches of symbolic policy learning are limited to learning static policies that have a fixed mapping from observations to control outputs [14, 17, 30, 26, 13, 38]. However, extending static policies to real-world scenarios

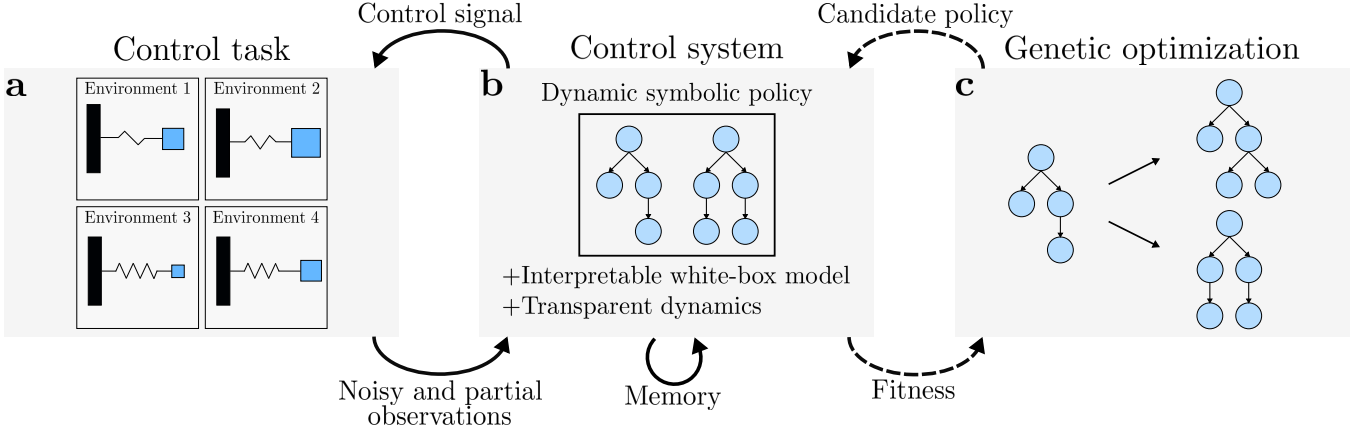


Figure 1: **The general framework for discovering dynamic symbolic policies with genetic programming.** (a) The control task to be solved by the control system. The parameters in the environment may differ in each trajectory, and the observations are partial. (b) The control system is a dynamic symbolic policy, defined by interpretable symbolic expressions. The control system has internal dynamics that function as memory. The control system receives observations from the environment and outputs a control signal. (c) The symbolic policies are optimised with genetic programming. Candidate policies are evolved and evaluated on the control task which returns a fitness score, indicating the quality of the policy.

is difficult, because environments can be volatile (change across time) or partially observable (providing noisy and limited information about the state of the environment). Dynamic policies could in principle solve these issues by incorporating memory to integrate past observations [16], but it is as of yet unclear how to optimise such policies in closed-loop control tasks, while incorporating interpretability.

Due to the non-differentiable structure of mathematical expressions, gradient-based methods cannot be used for the optimisation of symbolic policies. A viable alternative is genetic programming (GP), an evolutionary algorithm that learn computer programs [25]. GP has seen great successes in symbolic regression problems, which seek to discover interpretable mathematical models describing data [9, 35, 20, 37, 32, 6, 46]. Therefore we consider GP as a promising approach to optimise dynamic symbolic policies to solve control tasks [17, 30].

In the dynamic policies, the GP learns a symbolic representation of a state equation, describing the flow of a differential equation that takes observations as input and generates controls as output. Here, the latent state of the underlying differential equations functions as a memory system to capture long term dependencies in the data, which could improve the policy’s robustness and generalisability [16]. This is similar to the use of neural differential equations to estimate parameterized dynamical systems [10]. However, in contrast to neural differential equations we learn a symbolic, interpretable representation of the state equation that implements the policy.

In this paper, we introduce a method for evolving dynamic symbolic policies with GP to solve dynamic control tasks (Fig. 1). Using this approach, dynamic symbolic policies are successfully evolved in linear and non-linear environments, under several challenging circumstances such as partial observability and varying environment settings where static policies obtain limited performance. High-performing symbolic policies are still discovered when the control dimension increases, showing that our method is scalable. Furthermore, we find that the evolved symbolic policies obtain comparable performance as the black-box baseline, given by neural differential equations [10]. The key contribution of our work is a method for discovering interpretable high-performing dynamic symbolic policies with GP without requiring human expertise.

## 2 Methods

The goal of this paper is to evolve dynamic symbolic policies that obtain high performance in control problems. We compare dynamic symbolic policies with static symbolic policies, which are explained in more detail in this section. Afterwards, the specifics of the GP algorithm and how we extended GP to learn multiple trees efficiently are

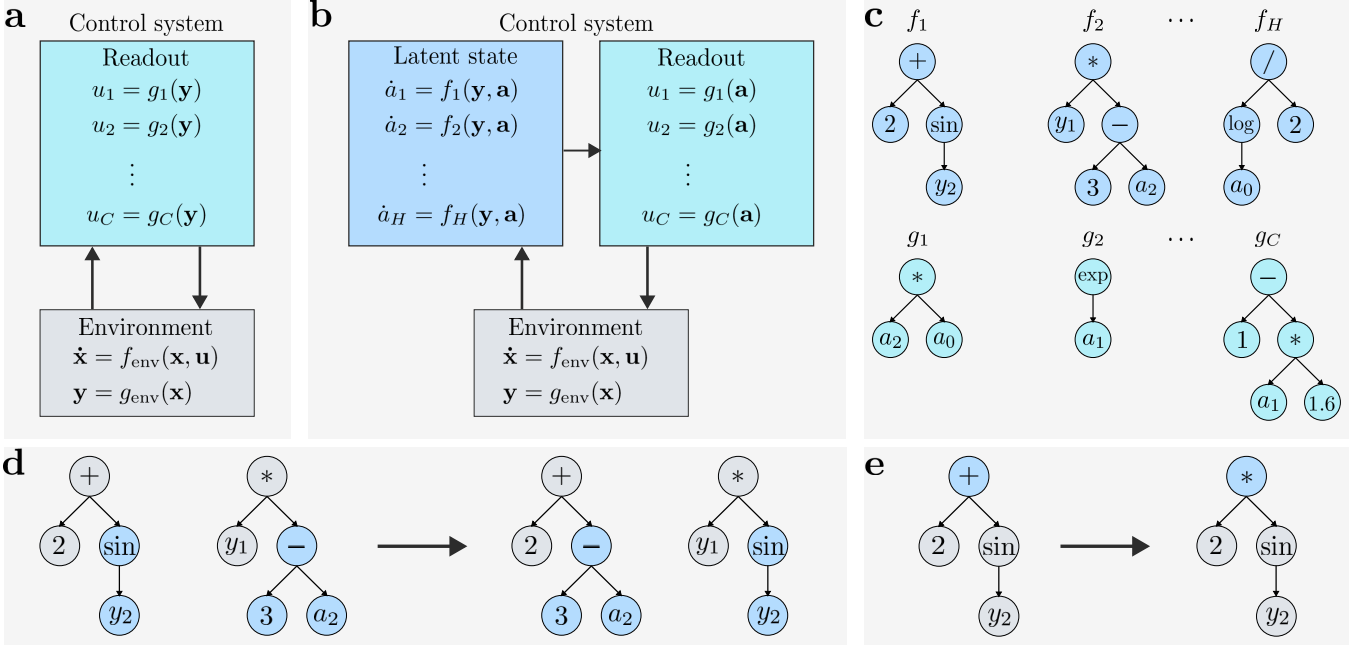


Figure 2: **Structure and optimisation of the static and dynamic symbolic policies.** (a) The feedback loop of an environment coupled with a control system that implements a static policy.  $C$  represents the number of control signals required to interact with the environment. For every function  $g_j$  a tree is optimised. (b) The control system is extended to include a latent state to implement a dynamic policy.  $H$  represents the number of units in the latent state. (c) An example representation of how a dynamic symbolic policy is represented by a set of trees. A tree is learned for every latent state and output signal. The functions  $f_i$  and  $g_j$  match the control system’s structure defined in panel b. The trees are optimised with genetic programming. (d) In genetic programming, crossover is applied to a pair of parents and produces two offspring individuals. The blue subtrees are interchanged between the two trees. (e) Mutation changes one individual and results in a single offspring. In this example, the blue node is a function node that is changed to a different type of function node.

described. In subsequent subsections the baselines and experiments we performed are detailed. The code including our GP implementation, environments and baselines is available at: <https://github.com/sdevries0/MultiTreeGP>.

## 2.1 Environment model

To evaluate a candidate symbolic policy proposed by GP, a coupled system consisting of the policy and an environment is simulated, as described in Fig. 2a and Fig. 2b. The environment is modeled by a state  $\mathbf{x} \in \mathbb{R}^N$ , following the dynamics of a stochastic differential equation

$$d\mathbf{x} = f_{\text{env}}(\mathbf{x}, \mathbf{u})dt + \mathbf{V}d\mathbf{w} \quad (1)$$

where  $\mathbf{u} \in \mathbb{R}^C$  is the control input,  $f_{\text{env}}$  is the environment’s state equation,  $\mathbf{w} \in \mathbb{R}^K$  is a multivariate Wiener process and  $\mathbf{V} \in \mathbb{R}^{N \times K}$  determines how the process noise influences the dynamics.

The controller receives observations  $\mathbf{y} \in \mathbb{R}^M$  from the state  $\mathbf{x}$ , determined by function  $g_{\text{env}}$  and possibly corrupted by noise. In our experiments, the noisy observations are generated by

$$\mathbf{y} = \mathbf{D}\mathbf{x} + \epsilon \quad (2)$$

where  $\mathbf{D} \in \mathbb{R}^{M \times N}$  is a readout matrix and  $\epsilon \sim \mathcal{N}(\mathbf{0}, \Sigma)$  is Gaussian observation noise. When relevant, the policy receives a target state  $\mathbf{x}^*$  that should be achieved in the environment. The policies are evaluated on a batch of trajectories, with a batch size of 32. In every trajectory, the initial conditions are randomly sampled, and if applicable target states and environment parameters are sampled.

## 2.2 Control model

**Static policies** Symbolic control systems are conventionally defined as static symbolic policies [26, 17, 14], which directly map observations to a control signal (Fig. 2a). The policy is represented as a function  $g$ , which computes the control signal with only the observations  $\mathbf{y}$  and potential target states  $\mathbf{x}^*$  as input. This setup is given by

$$u_j = g_j(\mathbf{y}, \mathbf{x}^*) \quad (3)$$

for  $1 \leq j \leq C$ .

**Dynamic policies** We extend this approach to dynamic symbolic policies (Fig. 2b), which include memory by using a latent state. The latent state processes incoming observations, and the readout function maps the latent state to a control signal. The dynamic policies contain expressions for the latent dimension and control dimension (Fig. 2c). The latent state is governed by a system of ordinary differential equation, according to

$$\dot{\mathbf{a}}_i = f_i(\mathbf{a}, \mathbf{y}, \mathbf{u}, \mathbf{x}^*) \quad (4)$$

for  $1 \leq i \leq H$ . Note that the dynamic policies also receive the previous control as an additional input. The readout functions of the dynamic policies are similar to Equation 3, but the input to  $g_j$  is given by the latent state  $\mathbf{a}$  instead of the observations  $\mathbf{y}$ . That is,

$$u_j = g_j(\mathbf{a}, \mathbf{x}^*) \quad (5)$$

for  $1 \leq j \leq C$ .

## 2.3 Numerical integration

Both the dynamics of the environment and the controller are simulated as a coupled system over a specified time range  $[t_0, t_f]$  with  $t_0$  the initial time and  $t_f$  the final time. For the environment and dynamic policies, we need to resort to numerical integration. To this end, we make use of the DiffraX library [23]. Because the systems are stochastic, the integration is performed using the Euler-Heun method with a fixed step size  $\Delta t$  [24]. This results in trajectories  $\mathbf{x}_{0:f} = (\mathbf{x}_0, \dots, \mathbf{x}_f)$  and  $\mathbf{u}_{0:f} = (\mathbf{u}_0, \dots, \mathbf{u}_f)$  with  $\mathbf{x}_i$  and  $\mathbf{u}_i$  the state and control at time  $t_i$ . These trajectories are used to determine the policy’s fitness using a fitness function  $F(\mathbf{x}_{0:f}, \mathbf{u}_{0:f})$ .

## 2.4 Genetic programming

The symbolic policies are evolved via genetic programming (GP). GP is a variant of evolutionary algorithms that focuses on learning computer programs [25]. A population of solutions is evolved to satisfy a certain goal or task through stochastic optimisation. In our setup, individuals are represented by tree-structured computational graphs, constructed from predefined sets of function nodes and leaf nodes. Function nodes cover mathematical operators and functions, while leaf nodes describe variables and constants. GP is largely defined by two hyperparameters. The first hyperparameter is the number of generations, which determines how many iterations of evolution are performed. The second hyperparameter is the population size, which defines the number of candidates that are evolved at every generation. See Algorithm 1 for an overview of the GP algorithm. The GP algorithm consists of initialisation, evaluation and reproduction steps, as described in more detail in the following sections.

### 2.4.1 Initialisation

Initially the population consists of randomly generated individuals, which will generally score poorly on the problem. Nonetheless, the initial population can already have a large effect on the success of the full algorithm [5]. The initial population should cover enough of the search space for the genetic operations to be useful. The initialisation strategy that was originally introduced is called Ramped Half-and-Half [25]. In this method, trees are either sampled fully, where leaf nodes can only appear at the maximum depth, or the trees grow randomly, which means that leaf nodes can appear at earlier depths, so that the initial population covers both shallow and deep trees.

### 2.4.2 Evaluation

To evaluate an individual, its tree is transformed into a program of desired functionality and tested on a problem. The performance of the individual is expressed with a fitness score, computed with a fitness function. The fitness scores are used to select individuals for reproduction, where fitter individuals produce more offspring. After evaluation, parents are selected for reproduction using tournament selection [11].

### 2.4.3 Reproduction

In GP, the new population is built with new candidate solutions that are generated with crossover and mutation. In crossover the genotype of two individuals are combined to produce new trees. Fitter individuals are more likely to be selected for reproduction, therefore the offspring is built from promising tree structures. In both parents a random node from the tree is selected, after which these nodes and their subtrees are swapped. An example of the crossover operator is shown in Fig. 2d. Uniform crossover is a variant of the standard crossover where multiple nodes can be swapped between a pair of trees without swapping full subtrees [39]. Uniform crossover improves the locality of the crossover operation, but both types of crossover can produce fit individuals and are therefore both included in our implementation.

Mutation was originally not integrated into GP [25], but mutation has shown to be a useful addition to the algorithm [29]. Mutation is applied to a single individual to generate one offspring and is applied instead of crossover in our implementation. Many aspects of trees can be mutated, for example changing, deleting or adding operators, replacing subtrees or changing variables or constants. Fig. 2e shows an example of mutation, in which an operator is changed to a different type of operator. Besides crossover and mutation, the new population also consists of randomly generated individuals and the fittest individuals from the previous generation.

The number of trees that has to be optimised differs for the static and dynamic policies. The static policies evolve a tree for every control input the problem requires. These trees also have to be evolved in the dynamic policies, but additional trees are optimised for every latent state variable. We chose to fix the size of the latent state in the dynamic policies and allow the readout function to learn which latent states to use. To learn both a symbolic latent state and readout function simultaneously in the dynamic policies, the individuals in the GP algorithm are extended to learn multiple trees [9]. During reproduction, crossover and mutation are not applied to every tree in the individual to be able to make small jumps through the search space. Crossover is only applied to trees in the same position in two parents, and a third type of crossover is introduced in which only complete trees are swapped between individuals.

### 2.4.4 Regularisation

Regularisation is necessary in GP to produce interpretable trees and improve the efficiency of the optimisation. To regularise the size and complexity of the reproduced trees, a punishment relative to the number of nodes in a tree is added to the fitness [28]. Additionally, the depth of the trees is limited to seven, and during initialisation the depth is set to four. To introduce more compact trees in the population, a small part of the population is simplified mathematically at every generation [19]. To improve diversity in the population during evolution, multiple subpopulations are evolved independently [12]. By configuring the hyperparameters in each subpopulation differently, exploration and exploitation is enforced explicitly [18]. Finally, dynamic policies with constant readout functions that only consist of targets or scalars and ignore the latent state, often form local minima because they offer stable solutions. However such policies will never come close to high-performing policies. To improve the efficiency of the evolutionary search, every readout function of a dynamic policy that is reproduced or sampled will have at least one reference to a latent variable to avoid such local minima, or else it is rejected for the next population.

## 2.5 Baselines

The static and dynamic symbolic policies generated with GP are compared with two baselines. The baselines are evaluated with the same population size and number of generations for every experiment.

The first baseline is random search of dynamic symbolic policies, which randomly samples a set of trees for each policy. The policies have the same model structure as the dynamic policies (Fig. 2c). The random search policies have the same number of trees in the latent state and are built from the same set of functions and leaf nodes as used in GP. The maximum depth of trees found with random search is fixed to seven. Random search is included

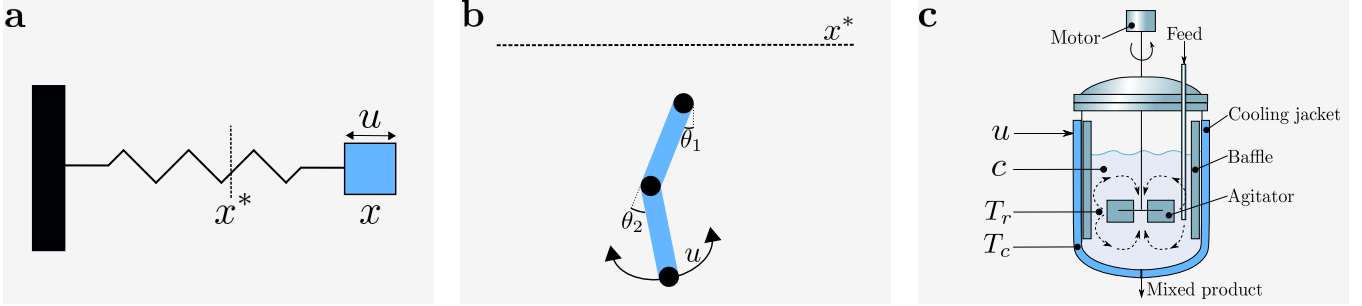


Figure 3: **Visualisations of the experiments.** (a) In the harmonic oscillator, the position of the oscillator  $x$  has to be moved to a target state  $x^*$  by applying the control force  $u$ . (b) The acrobot consists of two links, which are each defined by the angles  $\theta_1$  and  $\theta_2$ . To complete the swing up, the end of the second link has to be moved above the target height  $x^*$  by applying control force  $u$  on the second link. (c) The continuous stirred tank reactor is described by the concentration of reactant  $c$ , the temperature  $T_r$  in the main reactor, and the temperature  $T_c$  in the cooling jacket. The temperature in the reactor should be stabilised at a set point temperature  $T_r^*$ . The flow of coolant into the cooling jacket is controlled by  $u$ .

as a baseline to demonstrate if GP can find better solutions with less computation than random sampling, therefore showing the additional value of the genetic operators during optimisation.

To verify that the symbolic policies are high-performing, the symbolic policies are also compared to black-box policies modeled by neural differential equations (NDEs) [10]. The NDEs in our experiments implement Equations 4 and 5 using black-box neural networks. Specifically, we use

$$\dot{\mathbf{a}} = \tanh(\mathbf{A}\mathbf{z}) \quad (6)$$

with  $\mathbf{z} = (\mathbf{a}, \mathbf{y}, \mathbf{u}, \mathbf{x}^*, 1)$  a column vector concatenating the inputs and a constant, and  $\mathbf{A} \in \mathbb{R}^{N \times |\mathbf{z}|}$  a matrix. The linear readout layer is defined as

$$\mathbf{u} = \mathbf{B}\mathbf{v} \quad (7)$$

with  $\mathbf{v} = (\mathbf{a}, \mathbf{x}^*, 1)$  and  $\mathbf{B} \in \mathbb{R}^{C \times |\mathbf{v}|}$ . In this case, model parameters are optimised using covariance matrix adaption evolution strategies [15]. In all experiments, the dimension of  $\mathbf{a}$  was set to five for the NDE baseline. If policies discovered with GP can obtain similar fitness scores as the black-box NDE, the symbolic policies are said to be high-performing.

The performance of our method and the baselines is demonstrated through the best fitness at every generation during evolution, averaged over 20 independent evolutionary runs. The validation fitness of the best policy found in every run is displayed to confirm that the policies generalise to unseen conditions, but also to inspect the variance of convergence in the different evolutionary processes.

## 2.6 Environments

Our method and the baselines are evaluated on three different environments, as shown in Fig. 3. The first environment is the stochastic harmonic oscillator (SHO), which is a linear environment that can be solved with a linear controller. The policies are tested in a noisy setting, a partial observable setting where only a subset of the state variables is observed, and a setting where the environmental parameters vary. Here, an analytically optimal control policy, linear quadratic Gaussian (LQG) control, is used as an optimal baseline for comparison. The second environment is the acrobot swing up task with bounded continuous action space. This is a non-linear environment that requires a non-linear controller to perform the swing up. The policies solve the acrobot under noise and partial state observability. The third environment is the continuous stirred tank reactor (CSTR). The CSTR is a non-linear industrial system, which shows how well GP can find symbolic policies in an industrial setting. The parameters of the CSTR are varied in every trial and the state is partially observed. The chosen hyperparameter setting of the GP algorithm for each experiment are presented in Table 2 (Appendix 2.4). The choice of the function sets are described in the following subsections.

### 2.6.1 Stochastic harmonic oscillator

The SHO is a linear model that describes the position and velocity of an oscillating mass in a single dimension under random perturbations. The SHO is visualised in Fig. 3a and the dynamics of the SHO are given by

$$d\mathbf{x} = (\mathbf{A}\mathbf{x} + \mathbf{b}u)dt + \mathbf{v}dw \quad (8)$$

with

$$\mathbf{A} = \begin{bmatrix} 0 & 1 \\ -\omega & -\zeta \end{bmatrix}, \quad \mathbf{b} = \begin{bmatrix} 0 \\ 1 \end{bmatrix}, \quad \mathbf{v} = \begin{bmatrix} 0 \\ 0.05 \end{bmatrix}. \quad (9)$$

Depending on the choice of  $\omega$  and  $\zeta$  we obtain different harmonic oscillators, reflecting different choices of the oscillator’s mass, spring constant and damping.

The fitness function was chosen as the negative quadratic cost function, defined as

$$F(\mathbf{x}_{0:f}, \mathbf{u}_{0:f}) = - \sum_{t=0}^f (\mathbf{x}_t - \mathbf{x}^*)^\top \mathbf{Q} (\mathbf{x}_t - \mathbf{x}^*) - r u_t^2 \quad (10)$$

with  $\mathbf{Q} = \text{diag}(0.5, 0)$  and  $r = 0.5$ . Here,  $\mathbf{Q}$  punishes the policy for the distance between  $\mathbf{x}$  and some target state  $\mathbf{x}^*$  and  $r$  penalises the control strength. The initial condition  $\mathbf{x}_0$  is randomly sampled from a normal distribution with zero mean and variance  $\text{diag}(3, 1)$  for the position and velocity respectively. The target position is chosen randomly by sampling uniformly between -3 and 3 in each trial, while the target velocity is always set to zero. As the optimal LQG control is linear, the function set includes basic arithmetic operators.

GP and the baselines are tested on the SHO in three different experiments. In the first experiment the policies interact with the standard setting of the SHO. In this experiment  $\mathbf{A}$  is specified with  $\omega = 1$  and  $\zeta = 0$  and the state observations are noisy. In the second experiment the state of the SHO is partially observed, as the policies only observe the position while the velocity is unknown.  $\mathbf{A}$  remains the same in this experiment. In the third experiment, the policies are evaluated on generalisability. In each trial  $\omega$  and  $\zeta$  are different, specifically  $\omega \sim U(0, 2)$  and  $\zeta \sim U(0, 1.5)$ . In this experiment both the position and velocity are observed again. In the experiments with observation noise, the parameters of the readout function are set to  $\mathbf{D} = \mathbf{I}$  and  $\Sigma = 0.3\mathbf{I}$  (see Equation 2). In experiments with partial state observability,  $\mathbf{D}$  is adapted such that only the relevant observations are returned and the dimension of  $\Sigma$  is decreased to match the number of observations.

### 2.6.2 Acrobot swing up task

The acrobot is defined by two connected links, which is visualised in Fig. 3b. The first link is connected to a fixed position. In the swing up task, the goal of the policy is to bring the end point of the second link above a certain threshold height. The dynamics of the acrobot are defined as follows [40]. Let  $\theta_1$  and  $\theta_2$  denote the angles of the first and second link, respectively. Their dynamics are given by

$$\begin{aligned} \ddot{\theta}_1 &= -\frac{d_2 \ddot{\theta}_2 + \phi_1}{d_1} \\ \ddot{\theta}_2 &= \frac{u_1 + d_1^{-1} d_2 \phi_1 - m_2 l_1 l c_2 \dot{\theta}_1^2 \sin(\theta_2) - \phi_2}{m_2 l_{c2}^2 + I_2 - d_1^{-1} d_2^2} \end{aligned}$$

with parameters as defined in Appendix B. In the acrobot experiment that requires two control forces, the state equation of  $\dot{\theta}_1$  is adapted to  $\ddot{\theta}_1 = (u_2 - d_2 \ddot{\theta}_2 - \phi_1)/d_1$ . In practice, we convert this system to a stochastic first-order system

$$d\mathbf{x} = f(\mathbf{x}, \mathbf{u})dt + \mathbf{V}d\mathbf{w}$$

with  $\mathbf{x} = (\theta_1, \theta_2, \dot{\theta}_1, \dot{\theta}_2)^\top$  where  $\mathbf{V} = \text{diag}(0, 0, 0.05, 0.05)$  adds noise to the angle accelerations.

The fitness function is a sparse reward function with control regularisation, defined as

$$F(\mathbf{x}_{0:f}, \mathbf{u}_{0:f}) = -t_f - \sum_{t=0}^f \mathbf{u}_t^\top \mathbf{R} \mathbf{u}_t \quad (11)$$

where  $t_f$  describes the time point at which the swing up is accomplished. The control  $\mathbf{u}$  is clipped between -1 and 1, forcing policies to learn to build momentum to accomplish the swing up. The swing up is accomplished when  $-\cos(\theta_1) - \cos(\theta_1 + \theta_2) > x^*$ , where  $x^*$  is a fixed target height in every trial. Hence, the policy must try to minimise  $t_f$  and its control use.

In every experiment,  $\mathbf{R} \in \mathbb{R}^{C \times C}$  is set to  $0.01\mathbf{I}$ ,  $x^*$  to 1.5 and the initial states are sampled from  $U(-0.1, 0.1)$ . Observations of  $\theta_i$  are wrapped between  $[-\pi, \pi]$  and a trial terminates when  $\theta_1 > 8\pi$  or  $\theta_2 > 18\pi$ . Policies are discovered to solve the acrobot in three different experiments. In the first experiment the state of the acrobot is observable with noise and control force is only applied to the second link. In the second experiment the acrobot state is made partially observable, as the policies no longer observe the angular velocities. In the third experiment, the policies can apply independent forces to both links, and the angular velocities are observed again. The observations of the acrobot include angles, therefore the sine and cosine functions are added to the function set of the GP algorithm, besides the arithmetic operators. As for the SHO, the parameters of the readout function are set to  $\mathbf{D} = \mathbf{I}$  and  $\mathbf{\Sigma} = 0.3\mathbf{I}$  in case of observation noise. In experiment with partial state observability,  $\mathbf{D}$  is again changed to exclude the unobserved variables and  $\mathbf{\Sigma}$  is shrunken to the correct dimension.

### 2.6.3 Continuous stirred tank reactor

The CSTR describes a chemical process following non-linear dynamics [42]. The CSTR consists of a main tank that contains a mixture of chemicals and a cooling jacket around the main tank. A visualisation of the CSTR is presented in Fig. 3c. To optimise the chemical process inside the main tank, the temperature has to be stabilised around a setpoint temperature. The temperature in the cooling jacket can be influenced directly by altering the input flow of coolant, which in turn affects the temperature in the main tank. The dynamics of the CSTR are defined as in [4], extended with a Wiener process to incorporate stochasticity. Let  $\mathbf{x} = (c, T_r, T_c)^\top$ . The CSTR is defined as a stochastic first-order system

$$d\mathbf{x} = f(\mathbf{x}, \mathbf{u})dt + \mathbf{V}dw$$

with  $\mathbf{V} = \text{diag}(0.025, 3, 3)$ . The state equation is defined as  $f(\mathbf{x}, \mathbf{u}) = [f_1(\mathbf{x}, \mathbf{u}), f_2(\mathbf{x}, \mathbf{u}), f_3(\mathbf{x}, \mathbf{u})]^\top$  with

$$\begin{aligned} f_1(\mathbf{x}, \mathbf{u}) &= \frac{q_r}{V_r} (c_f - c) + k(T_r)c \\ f_2(\mathbf{x}, \mathbf{u}) &= \frac{q_r}{V_r} (T_f - T_r) + \frac{-\Delta H}{\rho C_p} k(T_r)c + \frac{UA}{\rho C_p V_r} (T_c - T_r) \\ f_3(\mathbf{x}, \mathbf{u}) &= \frac{q_c}{V_c} (T_{cf} - T_c) + \frac{UA}{\rho C_p V_r} (T_r - T_c) \end{aligned}$$

and the parameters as defined in Table 4.

The fitness function is chosen as the negative quadratic cost function, defined as

$$F(\mathbf{x}_{0:f}, \mathbf{u}_{0:f}) = - \sum_{t=0}^f (\mathbf{x}_t - \mathbf{x}^*)^\top \mathbf{Q} (\mathbf{x}_t - \mathbf{x}^*) - ru_t^2 \quad (12)$$

where

$$\mathbf{Q} = \begin{bmatrix} 0 & 0 & 0 \\ 0 & 0.01 & 0 \\ 0 & 0 & 0 \end{bmatrix}, \quad r = 0.0001, \quad \mathbf{x}^* = \begin{bmatrix} 0 \\ T_r^* \\ 0 \end{bmatrix}. \quad (13)$$

The policy has to minimise the distance between the temperature in the reactor and the setpoint temperature  $T_r^*$ , while also minimising the control, i.e. the coolant flowrate. Only a single experiment is performed regarding the CSTR. This experiment tests policies for their generalisability to an industrial environment. The parameters of the CSTR are different in each trial, to simulate as if the policy is operating in multiple scenarios. In total, eight parameters vary between trials (Table 4). Additionally, the concentration in the reactor is not observed, and the observations of the temperature in the reactor and cooling jacket are noisy. The function set of the GP algorithm is extended to include the exponential and logarithmic functions to aid expressions to deal with the values of the temperatures, which typically range between 200 and 600. To generate the observations,  $\mathbf{D}$  is defined such that the concentration is excluded from the observations and  $\mathbf{\Sigma} = 7.5\mathbf{I}$ .



### 3 Results

We present a GP method for finding high-performing dynamic symbolic policies for solving control problems. The performance of a policy is tested by controlling three common control benchmark systems (as explained in detail in Section 2.6). We investigate whether GP evolves successful control policies for linear and non-linear environments, different observability levels, as well as changing environment conditions and multiple control dimensions. We compare the resulting dynamic symbolic policies to static symbolic policies, optimal control (where possible), random search (RS), and to a reference black-box model (NDEs).

#### 3.1 Genetic programming evolves linear and non-linear symbolic policies

To study whether GP can successfully evolve dynamic symbolic policies, we first consider the SHO and acrobot environments with noisy full state observability (Fig. 4a,b). In the SHO, we consider the linear quadratic Gaussian (LQG) controller as the upper bound fitness (black curves). The fitness of random search improves during optimisation (purple curves), but does not converge near the upper bound nor the other methods. Random search does occasionally discover a policy that competes with the evolutionary approaches, but not consistently (purple dots). Moving forward, we will no longer consider random search as a baseline, but the results were similar across all tasks. NDEs converge to a high fitness quickly and consistently, approximating the upper bound fitness in the SHO (green curves and dots).

To validate that symbolic policies reach similar performance as the NDE, we first optimised static symbolic policies (blue curves). The initial fitness of GP-S begins close to the upper bound fitness in the SHO, which indicates that well-performing static policies exist in the initial population, which is a result of the small search space of GP-S. However, from there, GP is not able to evolve policies reaching the optimal fitness, indicating that static policies are not complex enough to match the optimal controller. Similarly, in the acrobot swing-up task, GP-S begins at a high fitness, but does not improve much during evolution. In both tasks, GP-S converges significantly higher than RS, but is outperformed by the NDE in terms of fitness.

We next evolved dynamic symbolic policies (orange curves). In both tasks, the fitness of GP-D begins significantly lower than GP-S, due to the larger search space. However, GP-D quickly converges to a higher fitness than GP-S, approximating the upper bound fitness in the SHO. This indicates that the internal dynamics are able to correct for the noisy observations. Both the GP-S and GP-D policies are highly consistent across trials, with GP-D producing slightly better policies (blue and orange dots).

Overall, these experiments demonstrate that static and dynamic symbolic policies are effectively optimised with GP, especially compared to random search. High-performing linear and non-linear policies are evolved that compete with the black-box NDE, although the NDE is more consistent.

#### 3.2 Dynamic symbolic policies remain robust under partial state observability

The previous experiments demonstrated that static and dynamic symbolic policies are successfully evolved for linear and non-linear settings. However, these experiments assumed the full state is observed, which may not be representative for real-life applications. We hypothesised that the memory in dynamic policies is particularly beneficial when confronted with partial state observations. To test this hypothesis, symbolic policies were evolved for the SHO and acrobot environments under partial state observability, where the velocities are not observed (Fig. 4c,d).

The SHO remains linear, therefore the LQG controller again represents the upper bound fitness (black curves). The NDE converges to a slightly lower fitness (green curves) compared to the experiments with full state observability. However, the NDE still consistently produced policies close to the upper bound in terms of performance, with a few policies that perform worse on the acrobot (green dots).

As hypothesised, GP-S converges to a substantially lower fitness than under full state observability (blue curves). Every static symbolic policy fails to satisfy the task when the velocity is not observed (blue dots). Differently from GP-S, high-performing dynamic symbolic policies are still successfully evolved (orange curves). GP-D converges to a similar fitness as the NDE in both environments. Additionally, the validation fitness is consistent, and some policies even perform better than the NDE policies (orange dots).

This experiment demonstrated that static symbolic policies perform poorly under partial state observability compared to the dynamic symbolic policies and NDE. This result can be contributed to the lack of memory in the static policies. Memory allows for estimation of the velocity, which enables policies to solve the SHO and acrobot

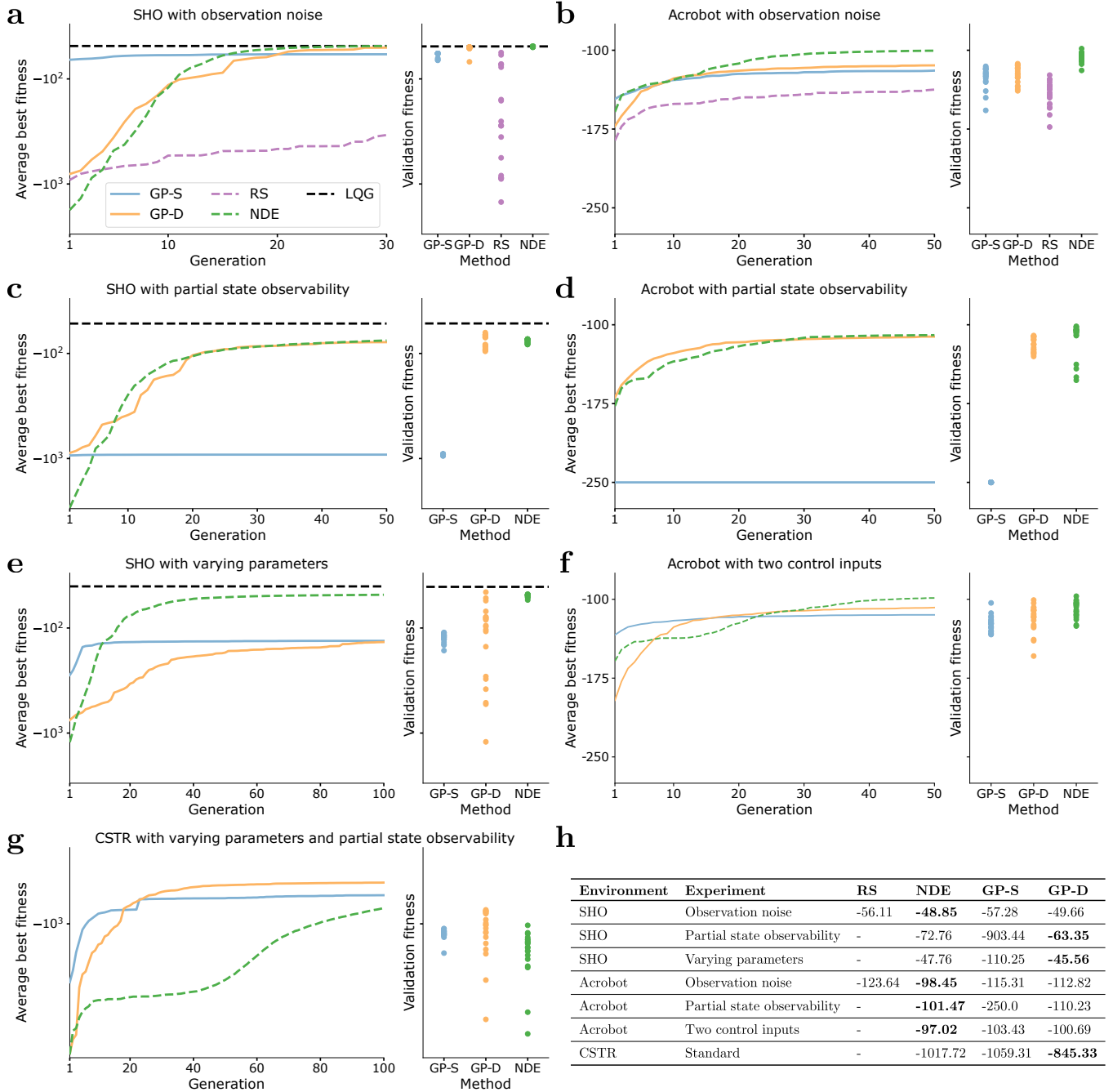


Figure 4: **Genetic programming evolves high-performing dynamic symbolic policies.** (a) Evolution results of the experiment on the stochastic harmonic oscillator (SHO) with observation noise. The left plot shows the best fitness at every generation during evolution, averaged over 20 independent runs. The methods included are genetic programming for static (GP-S) and dynamic (GP-D) policies, random search (RS), neural differential equation (NDE) and the analytical optimal linear quadratic Gaussian (LQG). The right plot presents the validation fitness obtained on unseen conditions with the best policy evolved in every evolutionary run. (b) Evolution results of the experiment on the acrobot with noisy observations. (c) Evolution results for the experiment in which the state of the SHO is partially observable. (d) Evolution results of the experiment on the acrobot under partial state observability. (e) Evolution results of the experiment on the SHO with varying parameters. (f) Evolution results of the experiment on the acrobot with two control inputs. (g) Evolution results of the experiment on the continuous stirred tank reactor (CSTR) with partial state observability and varying parameters. (h) Best fitness of each method on the validation set in each experiment. The bold fitness indicates a method is the best for an experiment.

tasks successfully. The latent state significantly increases the search space, but improves the robustness of the dynamic symbolic policies when confronted with partial observability.

### 3.3 Symbolic policies generalise to varying environments

Besides partial observations, realistic settings also require policies to generalise to varying and changing environments. To validate that generalising symbolic policies can be evolved, we test policies in the SHO with parameters that vary between trials (Fig. 4e). In this experiment, the upper bound fitness is again obtained with the LQG controller computed independently for each parameter setting (black curves). The NDE converges close to the upper bound fitness and is consistent across different runs (green curve and dots).

Static policies are first evolved to validate their generalisability (blue curve). GP-S does not converge near the upper bound fitness and the NDE. The validation fitness of the best static policies shows that a ceiling has been reached, as every policy is located close to the average (blue dots). GP-D converges to a similar fitness as GP-S (orange curve). However, the validation fitness of the dynamic symbolic policies shows an interesting pattern (orange dots). Many dynamic symbolic policies obtain a validation fitness that is better than any static policy, and some even compare with NDE policies. However, some dynamic symbolic policies obtain a validation fitness worse than any static policy.

The inconsistent evolution of dynamic symbolic policies is explained by the large search space. When dynamic policies are evolved successfully, they perform better than static policies. The memory allows dynamic policies to discover useful properties that increase generalisability. In our results, the majority of evolutionary runs resulted in dynamic policies that exceed the performance of static policies. Therefore the addition of the latent state in symbolic policies proves to be more beneficial than disadvantageous. Nonetheless, our approach does not consistently produce policies that perform comparably as the NDE.

### 3.4 Genetic programming evolves higher-dimensional policies

As the search space of symbolic policies is large, especially for the dynamic symbolic policies, it is important to validate whether high-performing are optimised efficiently when the control dimension increases. In this experiment, the policies can apply control forces to both links to accomplish the acrobot swing-up (Fig. 4f). The NDE converges to a slightly higher fitness during evolution than in the other experiments on the acrobot, because more force can be applied to solve the swing up (green curve). The best NDE policies obtain consistent validation fitness (green dots).

Our method is first tested to produce static symbolic policies with two control outputs (blue curve). The search space of static policies is still small compared to the dynamic policies, as is observed from the higher initial average best fitness compared to the other methods. The average best fitness of GP-S does not improve much during evolution, and converges at a worse fitness than the NDE. The validation fitness shows that most static policies perform similarly, but one evolved policy performs better than the other static policies (blue dots). GP-D converges at a slightly better fitness than GP-S, but worse than NDE (orange curve). The validation fitness obtained by dynamic symbolic policies mostly overlaps with that of the static symbolic policies and NDE policies, although a few policies are worse than any policy obtained by the other methods (orange dots). This experiment demonstrates that GP still evolves higher-dimensional control policies that accomplish the acrobot swing up, even though the size of the search space was increased even further.

### 3.5 Generalising symbolic policies are discovered for an industrial application

In the final experiment, we apply our method to the continuous stirred tank reactor (CSTR), an industrial problem. The temperature in the reactor has to be stabilised at a setpoint temperature by controlling the flow of coolant into the cooling jacket (Fig. 4g). To increase the complexity of the problem, the environment setting is varied between trials and the policies receive partial state observations.

The NDE has not converged after the dedicated number of generations, while being stuck at a poor fitness for the first half of the evolution (green curve). A potential reason for the limited convergence of the NDE could be that they cannot easily approximate the non-linearity required to stabilise the reactor efficiently. The validation fitness of the NDE policies is lower on average than the symbolic policies, and there are a few bad-performing policies (green dots).

Table 1: The best static and dynamic symbolic policies discovered with genetic programming for every experiment.  $u$  represents the function that outputs the control signal. In the dynamic policies, the functions of  $a_i$  represent the state equations of the latent variables. When a latent variable is not referred to in any of the other expressions, it is labelled as inactive.

Environment	Experiment	Static policy	Dynamic policy
SHO	Observation noise	$u = -0.61y_2 + x^*$	$u = -2a_1 + 2.60a_2 + x^*$ $\dot{a}_1 = y_2$ $\dot{a}_2 = -u + x^*$
SHO	Partial state observability	$u = 0.75x^* - 0.11$	$u = 0.45(a_1 + x^*)$ $\dot{a}_1 = 2a_2 - u + x^*$ $\dot{a}_2 = -a_2 - 0.99u + y_1$
SHO	Varying parameters	$u = -1.10y_1 - 0.73y_2 + 1.83x^* + 0.17$	$u = -a_1^3 - a_2 + x^*$ $\dot{a}_1 = 27.76(-a_1 + y_1 + y_2 - x^*)$ $\dot{a}_2 = 0.32a_1$
Acrobot	Observation noise	$u = -y_3 + 1.29 \sin(y_4)$	$u = 2a_2 - \cos(2a_1)$ $\dot{a}_1 = 2y_1 - 2y_2$ $\dot{a}_2 = 5.47 \sin(\sin(y_1))$
Acrobot	Partial state observability	No successful policies	$u = 1.87a_1 + \cos(a_2)$ $\dot{a}_1 = 2.06y_1$ $\dot{a}_2 = y_1 - 2.68$
Acrobot	Two control inputs	$u_1 = 0.64y_4 + \sin(y_4) - 0.04$ $u_2 = \sin(0.37y_3)$	$u_1 = 2.71 \cos(a_2 - 0.57)$ $u_2 = -a_2 - 1.48$ $\dot{a}_1 = -8.66a_1 + y_4$ (inactive) $\dot{a}_2 = -3.44y_2$ $\dot{a}_3 = y_3$ (inactive)
CSTR	Standard	$u = T_c^4(T_r^*)^{-3} - T_r$	$u = a_1^2 a_2 + 2a_1 \log(T_r^*)$ $\dot{a}_1 = (2.92 - a_1)(u_1 + 2.98)$ $\dot{a}_2 = (u_1 - a_2 + 2.37)(a_2 - T_r^* + T_r)$

GP-S converges to a higher fitness than NDE (blue curve), and the validation fitness shows high consistency among the policies (blue dots). GP-D obtains a better fitness than GP-S during evolution (orange curve). GP-D discovered several policies that outperform GP-S and NDE in terms of validation fitness (orange dots). However, the high-performing dynamic symbolic policies are again not consistently found, as some policies obtain a validation fitness significantly worse than any static policy.

The best static and dynamic policies are shown in Table 1 (CSTR, both Static and Dynamic). The evolved symbolic policies include non-linear terms such as logarithms and multiplications of different variables. Such complex non-linear features are more difficult to approximate for the NDE, given the number of neurons in the latent state of the NDE. Increasing the number of neurons would improve its capability to approximate any function, however the optimisation of the network would become less efficient, requiring more computation. GP evolves these non-linear functionalities easily, which highlights another advantage of our method.

### 3.6 The latent states in a dynamic symbolic policy are transparent

Across the experiments, GP was able to find successful dynamic symbolic policies. The best validation fitness obtained with each method is presented in Table 4h. GP-D is generally competitive with black-box NDEs, and outperforms the NDE in 3 out of 7 experiments. The best validation fitness of GP-D is higher than GP-S for every experiment. The dynamic symbolic policies compete with the black-box baseline, while consisting of interpretable mathematical expressions. The best static and dynamic symbolic policies are displayed in Table 1. Visualising the dynamic symbolic policies reveals that the latent states exhibits transparent properties that allow us to investigate how the memory is used to solve control tasks.

First, we investigated the functionality of the best policy evolved to stabilise the SHO with varying parameters

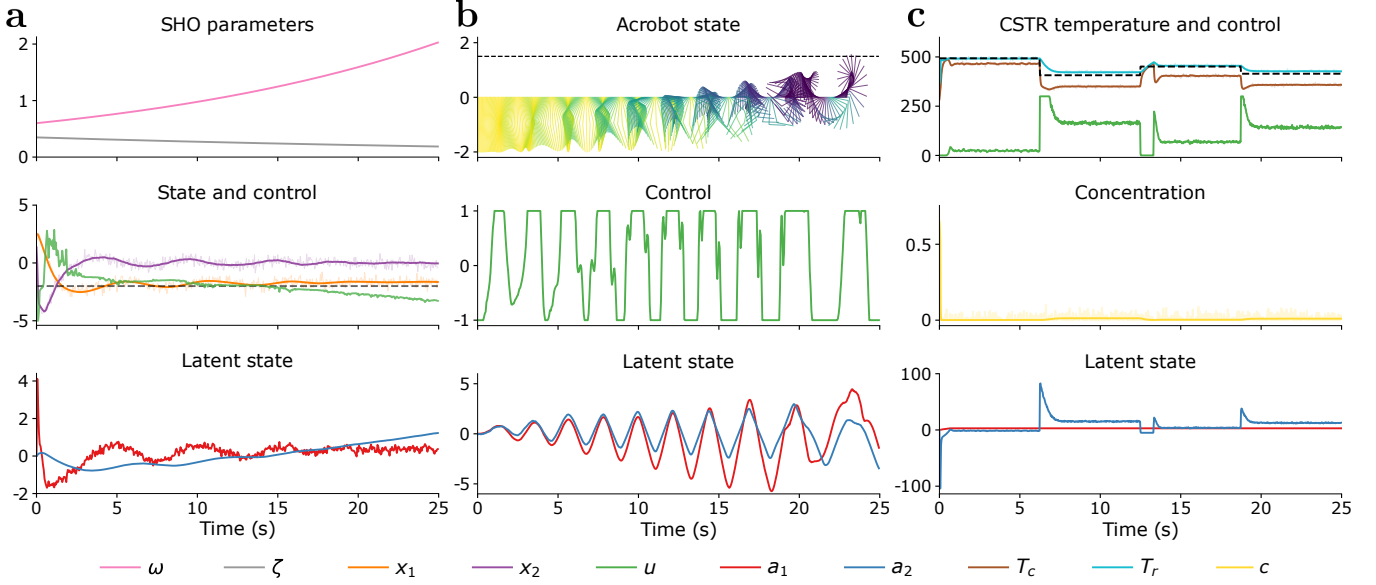


Figure 5: **Dynamic symbolic policies are transparent.** (a) Simulated trajectory of the stochastic harmonic oscillator (SHO) controlled by a dynamic symbolic policy. The parameters of the oscillator change over time, as is displayed in the top row. The plot in the second row shows the state and control in the trajectory. The shaded area around the states is observed by the policy. For each environment, the dashed line indicates the setpoint. The latent state variables of the policy are presented in the bottom row. The policy used in this simulation is described in Table 1 (SHO, Varying parameters, Dynamic) (b) A simulated trajectory of the acrobot with observation noise, where a dynamic symbolic policies applies force the second link. The top row shows the position of the two links over time. The second row presents the control force, and the bottom row shows the latent state variables. The policy is described in Table 1 (Acrobot, Observation noise, Dynamic). (c) Simulated trajectory of the CSTR controlled with a dynamic symbolic policy. The top row shows the temperature of the reactor and cooling jacket when the policy controls the coolant inflow with varying setpoint temperatures. The second row presents the concentration of the reactant in the reactor. The bottom row shows the behavior of the latent state of the policy. The policy used in this simulation is described in Table 1 (CSTR, Dynamic).

settings (Table 1, SHO, Varying parameters, Dynamic). Our interpretation of the symbolic expression of variable  $a_1$  is that it computes the distance between the target and position, adds the velocity and subtracts itself to decrease the influence of the noisy observations. Variable  $a_2$  integrates  $a_1$  multiplied with a constant, which we interpret as the estimate of the cumulative error. The readout subtracts  $a_2$  and the cube of  $a_1$  from the target state to output the policy’s control.

To demonstrate the generalisability of this policy within a single trial, we change the parameters of the SHO during the experiment (Fig. 5a, top row). The policy manages to keep the state close to the target state by increasing the strength of its negative control signal (Fig. 5a, middle row). Variable  $a_1$  initially fluctuates until the position is stabilised close to the target, where after it stays close to the origin (Fig. 5a, bottom row, red curve). Variable  $a_2$  first decreases, but increases during the trajectory to adjust to the changes in the environment, which causes the control force to increase (Fig. 5a, bottom row, blue curve).

The latent state should remain transparent when a policy becomes non-linear to still offer interpretability in more complex tasks than the SHO. To demonstrate the transparency in non-linear policies, the best policy obtained from acrobot swing-up task with observation noise is analysed (Table 1, Acrobot, Observation noise, Dynamic). Variable  $a_1$  computes the difference between the angles of the two links. Variable  $a_2$  inputs the angle of the first link in two nested sine functions, multiplied with a scalar. The readout subtracts the cosine of  $a_1$  from  $a_2$ . Our interpretation of this policy is that it applies force in the direction of the first link compared to the centre point to build momentum, and increases the force when the two links are not closely aligned to add extra momentum to the second link, resembling a bang-bang controller.

The mathematical expressions of the non-linear policy are less straightforward to interpret than the linear policy. Analysing the latent state of this policy helps with understanding the functioning of this policy. The policy quickly accomplishes the swing up of the acrobat (Fig. 5b, top row). The control force applied by the policy shows expected behaviour, switching between -1 and 1 to build momentum, and remains constant longer when the second link is close to the threshold height (Fig. 5b, middle row). The latent state shows similar behaviour, although variable  $a_1$  fluctuates with a higher amplitude (Fig. 5b, bottom row). The latent states are not as expressive as in the policy in Fig. 5a, and it is difficult to understand the individual contribution of each variable. Nonetheless, there is still more transparency in these dynamics than in a black-box policy.

For application purposes, it is also relevant that policies remain interpretable in an industrial setting, such as the CSTR. The best policy discovered for stabilising the CSTR is analysed for transparency (Table 1 CSTR, Dynamic). We interpret the state equation of variable  $a_1$  as a scaling factor that converges to 2.92 during the trajectory. The state equation of variable  $a_2$  computes the error between the temperature and setpoint, and adds a self-connection to improve robustness to noise. The error estimate is scaled by the sum of the control,  $a_2$  and a constant. The readout scales  $a_2$  with the squared of  $a_1$ , and adds a multiplication of  $a_1$  with the logarithm of the setpoint temperature. The control therefore reacts to differences between the setpoint and current temperature, scaled increasingly during the trajectory.

To increase the number of responses in the trial, the setpoint temperature is changed several times during the trajectory. The policy efficiently stabilises the temperature at each setpoint temperature (Fig. 5c, top row). The control signal reacts when the setpoint temperature changes, and remains close to zero when the temperature has to increase. The concentration of the reactant in the main reactor goes to zero quickly and only slightly increases when the control input changes (Fig. 5c, middle row). Variable  $a_1$  converges to 2.92 as expected (Fig. 5c, bottom row, red curve), while  $a_2$  shows large responses when the setpoint temperature changes (Fig. 5c, bottom row, blue curve). Together, the latent variables allow the policy to change its control output accordingly.

These example trials demonstrate that the dynamic symbolic policies are not only interpretable, but also offer transparency in the latent states. The latent state variables vary in their level of expressiveness, but overall analysing the latent state aids with understanding the functionality of a policy. The latent state showed to be beneficial for the robustness of a policy, however it also further improves the interpretability of symbolic policies.

## 4 Discussion

In this paper, we discovered interpretable and high-performing white-box control systems to solve control problems. The conventional approach is to find static symbolic policies, but these are difficult to extend to real-world challenges like partial observability and volatility. To improve the robustness of control systems, we evolved dynamic symbolic policies with memory with genetic programming (GP). The dynamic policies successfully solved control tasks with noisy and partial state observations, where the static policies failed to solve the task. Furthermore, dynamic symbolic policies generalise better to tasks with varying environment settings than static policies. These results show the benefits of the memory in the dynamic symbolic policies, and these policies can still be evolved efficiently with GP in terms of generations and population size. The symbolic policies were compared with a neural differential equation optimised with covariance-matrix adaptation evolution strategies as a proven black-box baseline [36]. The results demonstrate that dynamic symbolic policies are evolved that generally obtain comparable performance as the black-box baseline, although competitive symbolic policies are not consistently found across evolutionary runs.

Besides adequately solving control tasks, the dynamic symbolic policies have other advantages, such as that they consist of interpretable expressions and display transparent dynamics, as demonstrated in Fig. 5. These features help understanding the functioning of control systems, therefore contributing to identification of undesired behaviour. Additionally, the interpretability allows us to learn new approaches to solve tasks from the policies. To further increase the interpretability in the dynamic symbolic policies, the readout could be learned as a numerical vector that maps the latent state to a control signal. This way, all non-linear functionality is evolved in the latent state, and the relation between the latent state and control signal becomes easier to understand, which is currently not always trivial (Table 1). The consistency of evolution also improves, as less trees have to be optimised with GP, although another method for optimising the readout vector should be introduced.

The major limitation of evolving dynamic symbolic policies with GP, is the huge search space that has to be traversed, which hinders consistent evolution of high-performing policies. The results showed that GP converges faster and more consistently when static policies are evolved under standard environment circumstances. The search

space will grow even larger when the control problem contains higher-dimensional observation and control spaces. Our method demonstrated to be scalable when the environment required two control outputs (Fig. 4f), but this may not hold for more complex problems. Better policies can be evolved with GP when a higher population size and number of generations are selected, which also increases the computation requirements. However, previous research has focused extensively on improving the optimisation efficiency of GP, by integrating features such as optimisation of constants [41], semantic reproduction [43], population diversity control [7] and self-adaptation of hyperparameters [2].

Besides introducing the concept of dynamic symbolic policies, this research also resulted in a general GP framework that is not limited to optimisation of dynamic symbolic policy. First of all, other structures of symbolic policies can be configured, with the possibility to explicitly define different types of trees with unique inputs and functionality in the policy. Furthermore, the framework could also be used problems outside control, for example symbolic regression [6], discovering learning rules [21] or other directions within scientific discovery [45, 44, 33].

The memory in dynamic policies demonstrated to improve the generalisability to different parameter settings in an environment. However, this could be further extended to evolve a single policy that can solve different control problems, which relates to meta-learning. In [22], genetic programming is used to construct a memory-based agent that solves six different control problems under partial state observability, which has to recognize the task at hand purely from the observations. Our work could be integrated to replace the model of the agent with a dynamic symbolic policy. The interpretable policy expression and transparent latent state would aid in understanding how the agent solves different tasks with the same policy.

We conclude that the use of genetic programming is a viable route towards learning interpretable, efficient and robust dynamic symbolic policies for solving control tasks. We hope that this adds an important tool to the practitioners' toolbox in the endeavour to create trustworthy AI systems.

## Acknowledgements

This publication is part of the project ROBUST: Trustworthy AI-based Systems for Sustainable Growth with project number KICH3.L TP.20.006, which is (partly) financed by the Dutch Research Council (NWO), ASMPPT, and the Dutch Ministry of Economic Affairs and Climate Policy (EZK) under the program LTP KIC 2020-2023. All content represents the opinion of the authors, which is not necessarily shared or endorsed by their respective employers and/or sponsors.

## References

- [1] Amina Adadi and Mohammed Berrada. "Peeking inside the black-box: a survey on explainable artificial intelligence (XAI)". In: *IEEE Access* 6 (2018), pp. 52138–52160.
- [2] Peter J Angeline. "Two self-adaptive crossover operators for genetic programming". In: *Advances in Genetic Programming* (1996), pp. 89–109.
- [3] Anuradha M Annaswamy, Karl H Johansson, and George J Pappas. "2030 Control for Societal-Scale Challenges: Road Map". In: *IEEE Control Systems Society* (2023).
- [4] Rita Antonelli and Alessandro Astolfi. "Continuous stirred tank reactors: easy to stabilise?" In: *Automatica* 39.10 (2003), pp. 1817–1827.
- [5] Lawrence Beadle and Colin G Johnson. "Semantic analysis of program initialisation in genetic programming". In: *Genetic Programming and Evolvable Machines* 10 (2009), pp. 307–337.
- [6] Josh Bongard and Hod Lipson. "Automated reverse engineering of nonlinear dynamical systems". In: *Proceedings of the National Academy of Sciences* 104.24 (2007), pp. 9943–9948.
- [7] Edmund K Burke, Steven Gustafson, and Graham Kendall. "Diversity in genetic programming: An analysis of measures and correlation with fitness". In: *IEEE Transactions on Evolutionary Computation* 8.1 (2004), pp. 47–62.
- [8] Roberta Calegari, Giovanni Ciatto, and Andrea Omicini. "On the integration of symbolic and sub-symbolic techniques for XAI: A survey". In: *Intelligenza Artificiale* 14.1 (2020), pp. 7–32.
- [9] Hongqing Cao et al. "Evolutionary modeling of systems of ordinary differential equations with genetic programming". In: *Genetic Programming and Evolvable Machines* 1 (2000), pp. 309–337.

- [10] Ricky TQ Chen et al. “Neural ordinary differential equations”. In: *Advances in Neural Information Processing Systems* 31 (2018).
- [11] Yongsheng Fang and Jun Li. “A review of tournament selection in genetic programming”. In: *International Symposium on Intelligence Computation and Applications*. Springer. 2010, pp. 181–192.
- [12] Francisco Fernandez, Marco Tomassini, and Leonardo Vanneschi. “An empirical study of multipopulation genetic programming”. In: *Genetic Programming and Evolvable Machines* 4 (2003), pp. 21–51.
- [13] Jianping Gou et al. “Knowledge distillation: A survey”. In: *International Journal of Computer Vision* 129.6 (2021), pp. 1789–1819.
- [14] Jiaming Guo et al. “Efficient Symbolic Policy Learning with Differentiable Symbolic Expression”. In: *Advances in Neural Information Processing Systems* 36 (2024).
- [15] Nikolaus Hansen. “The CMA evolution strategy: A tutorial”. In: (2016). Preprint at <https://arXiv.org/abs/1604.00772>.
- [16] Nicolas Heess et al. “Memory-based control with recurrent neural networks”. In: (2015). Preprint at <https://arXiv.org/abs/1512.04455>.
- [17] Daniel Hein, Steffen Udluft, and Thomas A Runkler. “Interpretable policies for reinforcement learning by genetic programming”. In: *Engineering Applications of Artificial Intelligence* 76 (2018), pp. 158–169.
- [18] Francisco Herrera and Manuel Lozano. “Gradual distributed real-coded genetic algorithms”. In: *IEEE Transactions on Evolutionary Computation* 4.1 (2000), pp. 43–63.
- [19] Dale C Hooper and Nicholas S Flann. “Improving the accuracy and robustness of genetic programming through expression simplification”. In: *Proceedings of the 1st Annual Conference on Genetic Programming*. 1996, pp. 428–428.
- [20] Hitoshi Iba. “Inference of differential equation models by genetic programming”. In: *Information Sciences* 178.23 (2008), pp. 4453–4468.
- [21] Jakob Jordan et al. “Evolving interpretable plasticity for spiking networks”. In: *Elife* 10 (2021), e66273.
- [22] Stephen Kelly et al. “Evolving hierarchical memory-prediction machines in multi-task reinforcement learning”. In: *Genetic Programming and Evolvable Machines* 22 (2021), pp. 573–605.
- [23] Patrick Kidger. “On Neural Differential Equations”. PhD thesis. University of Oxford, 2021.
- [24] P.E. Kloeden, E. Platen, and H. Schurz. *Numerical Solution of SDE through Computer Experiments*. Springer, 1994.
- [25] John R Koza. “Genetic programming as a means for programming computers by natural selection”. In: *Statistics and Computing* 4 (1994), pp. 87–112.
- [26] Mikel Landajuela et al. “Discovering symbolic policies with deep reinforcement learning”. In: *International Conference on Machine Learning*. PMLR. 2021, pp. 5979–5989.
- [27] Octavio Loyola-Gonzalez. “Black-box vs. white-box: Understanding their advantages and weaknesses from a practical point of view”. In: *IEEE Access* 7 (2019), pp. 154096–154113.
- [28] Sean Luke and Liviu Panait. “A comparison of bloat control methods for genetic programming”. In: *Evolutionary Computation* 14.3 (2006), pp. 309–344.
- [29] Sean Luke and Lee Spector. “A comparison of crossover and mutation in genetic programming”. In: *Genetic Programming* 97 (1997), pp. 240–248.
- [30] Giorgia Nadizar, Eric Medvet, and Dennis G Wilson. “Naturally Interpretable Control Policies via Graph-Based Genetic Programming”. In: *European Conference on Genetic Programming (Part of EvoStar)*. Springer. 2024, pp. 73–89.
- [31] Erika Puiutta and Eric MSP Veith. “Explainable reinforcement learning: A survey”. In: *International Cross-Domain Conference for Machine Learning and Knowledge Extraction*. Springer. 2020, pp. 77–95.
- [32] Markus Quade et al. “Prediction of dynamical systems by symbolic regression”. In: *Physical Review E* 94.1 (2016), p. 012214.



- [33] Christopher Rackauckas et al. “Universal differential equations for scientific machine learning”. In: (2020). Preprint at <https://arXiv.org/abs/2001.04385>.
- [34] Gabrielle Ras et al. “Explainable deep learning: A field guide for the uninitiated”. In: *Journal of Artificial Intelligence Research* 73 (2022), pp. 329–396.
- [35] Erina Sakamoto and Hitoshi Iba. “Inferring a system of differential equations for a gene regulatory network by using genetic programming”. In: *Proceedings of the 2001 Congress on Evolutionary Computation (IEEE Cat. No. 01TH8546)*. Vol. 1. IEEE. 2001, pp. 720–726.
- [36] Tim Salimans et al. “Evolution strategies as a scalable alternative to reinforcement learning”. In: (2017). Preprint at <https://arXiv.org/abs/1703.03864>.
- [37] Michael Schmidt and Hod Lipson. “Distilling free-form natural laws from experimental data”. In: *Science* 324.5923 (2009), pp. 81–85.
- [38] Hiroaki Shimooka and Yoshiji Fujimoto. “Generating robust control equations with genetic programming for control of a rolling inverted pendulum”. In: *Proceedings of the 2nd Annual Conference on Genetic and Evolutionary Computation*. Citeseer. 2000, pp. 491–495.
- [39] William M Spears and Vic Anand. “A study of crossover operators in genetic programming”. In: *International Symposium on Methodologies for Intelligent Systems*. Springer. 1991, pp. 409–418.
- [40] Richard S Sutton. “Generalization in reinforcement learning: Successful examples using sparse coarse coding”. In: *Advances in Neural Information Processing Systems* 8 (1995).
- [41] Alexander Topchy, William F Punch, et al. “Faster genetic programming based on local gradient search of numeric leaf values”. In: *Proceedings of the Genetic and Evolutionary Computation Conference (GECCO-2001)*. Vol. 155162. Morgan Kaufmann San Francisco, CA. 2001.
- [42] Ashok Uppal, Willis Harmon Ray, and Aubrey B Poore. “On the dynamic behavior of continuous stirred tank reactors”. In: *Chemical Engineering Science* 29.4 (1974), pp. 967–985.
- [43] Leonardo Vanneschi, Mauro Castelli, and Sara Silva. “A survey of semantic methods in genetic programming”. In: *Genetic Programming and Evolvable Machines* 15 (2014), pp. 195–214.
- [44] Ricardo Vinuesa et al. “Opportunities for machine learning in scientific discovery”. In: (2024). Preprint at <https://arXiv.org/abs/2405.04161>.
- [45] Hanchen Wang et al. “Scientific discovery in the age of artificial intelligence”. In: *Nature* 620.7972 (2023), pp. 47–60.
- [46] Yiqun Wang, Nicholas Wagner, and James M Rondinelli. “Symbolic regression in materials science”. In: *MRS Communications* 9.3 (2019), pp. 793–805.
- [47] Yu Zhang et al. “A survey on neural network interpretability”. In: *IEEE Transactions on Emerging Topics in Computational Intelligence* 5.5 (2021), pp. 726–742.

# Appendices

## A Genetic programming

Our implementation of genetic programming followed Algorithm 1. The hyperparameters and function sets we used in each experiment are presented in Table 2. The choice for the population size and number of generations (see Section 2.4) were chosen to balance efficiency and consistent convergence empirically. The elite percentage was set to 0.1 in every experiment. The choice of the function sets are explained in the corresponding environment sections.

---

### Algorithm 1 Genetic programming algorithm

---

**Input** Number of generations  $G$ , population size  $N$ , elite percentage  $E$ , fitness function  $F$

```

1: initialise population  $P$  with size  $N$  (Section 2.4.1)
2: for  $g$  in  $G$  do
3:   evaluate each individual in  $P$  on  $F$  (Section 2.4.2)
4:   offspring  $O \leftarrow \{\}$ 
5:   append fittest  $E$  of  $P$  to  $O$ 
6:   while  $\text{size}(O) < N$  do
7:     randomly select reproduce from {crossover, mutation, simplification, sample}
8:     randomly select parents  $p$  from  $P$  with tournament selection
9:     children  $c = \text{reproduce}(p)$  (Section 2.4.3)
10:    append  $c$  to  $O$ 
11:   end while
12:    $P \leftarrow O$ 
13: end for
14: return fittest individual in  $P$ 

```

---

Table 2: Hyperparameters and function sets of the genetic programming algorithm used in every experiment.

Hyperparameter	SHO			Acrobot		CSTR
	Exp 1	Exp 2	Exp 3	Exp 1	Exp 2	Exp 1
Population Size	500	500	1000	500	500	1000
Number of Generations	30	50	100	50	50	100
Latent state size	2	2	2	2	2	2
Function set	+, -, *, /, power			+, -, *, /, power, sin, cos		+, -, *, /, power, exp, log

## B Acrobot parameters

The acrobot dynamics are defined in terms of the variables

$$\begin{aligned}
 d_1 &= m_1 l_{c1}^2 + m_2 (l_1^2 + l_{c2}^2 + 2l_1 l_{c2} \cos(\theta_2)) + I_1 + I_2 \\
 d_2 &= m_2 (l_{c2}^2 + l_1 l_{c2} \cos(\theta_2)) + I_2 \\
 \phi_1 &= -m_2 l_1 l_{c2} \dot{\theta}_2^2 \cos(\theta_2) - 2m_2 l_1 l_{c2} \dot{\theta}_2 \dot{\theta}_1 \sin(\theta_2) + (m_1 l_{c1} + m_2 l_1) g \cos\left(\theta_1 - \frac{\pi}{2}\right) + \phi_2 \\
 \phi_2 &= m_2 l_{c2} g \cos\left(\theta_1 + \theta_2 - \frac{\pi}{2}\right)
 \end{aligned}$$

with parameters of the system as shown in Table 3.

Table 3: Parameters of the acrobot swing up task.

Parameter	Unit	Description	Value or Range
$\theta_i$	rad	Angle of a link	$\theta_i(0) \sim U(-0.1, 0.1)$
$\dot{\theta}_i$	rad s <sup>-1</sup>	Angular velocity of a link	$\dot{\theta}_i(0) \sim U(-0.1, 0.1)$
$l_i$	m	Length of a link	1.0
$m_i$	kg	Mass of a link	1.0
$l_{ci}$	m	Position of the center of mass of a link	0.5
$I_i$	kg <sup>2</sup> m	Moment of inertia of a link	1.0
$g$	m s <sup>-2</sup>	Gravity	9.81

## C Continuous stirred tank reactor parameters

The descriptions of each parameter in the CSTR dynamics are shown in Table 4. Table 4 also contains the value, initial condition or sample range for each parameter. The variables that are indicated with a range are uniformly sampled within this range in every trajectory. The initial conditions of  $c$ ,  $T_r$  and  $T_c$  are uniformly sampled from the given distribution. The controlled parameter is clipped between 0 and 300. The reaction rate is defined as  $k(T_r) = k_0 \exp(-E/RT_r)$ .

Table 4: Parameters of the continuous stirred tank reactor. Each parameter is either set to a value, a function or sampled uniformly given a range.

Parameter	Unit	Description	Value or Range
$c$	mol L <sup>-1</sup>	Reactant concentration	$c(0) \sim U(0.5, 1.0)$
$T_r$	K	Reactor temperature	$T(0) \sim U(350, 375)$
$T_c$	K	Cooling jacket temperature	$T_c(0) \sim U(275, 300)$
$T_r^*$	K	Setpoint temperature	{400, 500}
$q_r$	L min <sup>-1</sup>	Feed flowrate of reactant into reactor	{75, 125}
$q_c$	L min <sup>-1</sup>	Feed flowrate of coolant into cooling jacket	Controlled parameter
$c_f$	mol L <sup>-1</sup>	Feed concentration of reactant into reactor	1
$T_f$	K	Feed temperature of reactant into reactor	{300, 350}
$T_{cf}$	K	Feed temperature of coolant into cooling jacket	{250, 300}
$V_r$	L	Volume of reactor	{75, 150}
$V_c$	L	Volume of cooling jacket	{10, 30}
$\Delta H$	J mol <sup>-1</sup>	Enthalpy of reaction	{-55 000, -45 000}
$\rho$	g L <sup>-1</sup>	Density	1000
$C_p$	J g <sup>-1</sup> K <sup>-1</sup>	Heat capacity	{0.2, 0.35}
$UA$	J min <sup>-1</sup> K <sup>-1</sup>	Heat transfer coefficient	{25 000, 75 000}
$k_0$	1/min	Arrhenius pre-exponential	$7.2 \times 10^{10}$
$E$	J mol <sup>-1</sup>	Activation energy	72 750
$R$	J mol <sup>-1</sup> K <sup>-1</sup>	Gas constant	8.314
$k(T_r)$	1/min	Reaction rate	Function of temperature